Energy dependence of the astrophysical *S* factor for the ^{6}Li$(p,\gamma)^7$Be reaction

R. M. Prior,[1,2] M. C. Spraker,[1,2] A. M. Amthor,[1] K. J. Keeter,[2,3] S. O. Nelson,[2,4] A. Sabourov,[2,4] K. Sabourov,[2,4] A. Tonchev,[2,4] M. Ahmed,[2,4] J. H. Kelley,[2,5] D. R. Tilley,[2,5] H. R. Weller,[2,4] and H. M. Hofmann[6]

[1]*Department of Physics, North Georgia College and State University, Dahlonega, Georgia 30597, USA*

[2]*Triangle Universities Nuclear Laboratory, Duke Station, Durham, North Carolina 27708, USA*

[3]*Department of Physics, Idaho State University, Pocatello, Idaho 83209, USA*

[4]*Department of Physics, Duke University, Durham, North Carolina 27708, USA*

[5]*Department of Physics, North Carolina State University, Raleigh, North Carolina 27695, USA*

[6]*Institut fur Theoretische Physik der Universitat Erlangen-Nurnberg, 91058 Erlangen, Germany*

(Received 13 August 2004; published 5 November 2004)

Polarized proton beams with energies from 80 to 130 keV have been used to determine the slope of the astrophysical *S* factor for the ^{6}Li$(p,\gamma_0)^7$Be and ^{6}Li$(p,\gamma_1)^7$Be reactions. The slope was determined from the relative yields at five incident proton energies. The slope of the *S* factor was found to be negative. The analyzing power measurements indicate that the reaction proceeds predominately by *s*-wave capture. The negative slope does not appear to be due to low-binding-energy effects, the effects of nearby resonances, or electron screening of the nuclei. A resonating group model calculation demonstrates a new mechanism for producing a negative slope at astrophysically relevant energies in radiative capture reactions.

DOI: 10.1103/PhysRevC.70.055801 PACS number(s): 25.40.Lw, 27.20.+n, 24.70.+s, 26.20.+f

I. INTRODUCTION

The low-energy behavior of many proton radiative capture reactions is important in nuclear astrophysics. In many cases, the cross sections at the energies of interest (in the so-called Gamow window) are not directly measured because the cross sections are extremely small. The needed cross sections must be obtained by extrapolating measured values at higher energies to very low energies. The extrapolation is usually performed using the astrophysical *S* factor, which removes the rapidly changing part of the cross section arising from penetrating the Coulomb barrier. Knowledge of the rate of change of the *S* factor with energy at very low energies is needed to perform a reliable extrapolation. Although this is frequently determined by the use of a direct-capture-model calculation, there are cases when this does not suffice. Low-energy resonances or subthreshold states can affect the extrapolation. In this work the results of a measurement of the slope of the astrophysical *S* factor for the ^{6}Li$(p,\gamma)^7$Be reaction are reported, and a new mechanism is introduced to explain the observed slope.

The ^{6}Li$(\vec{p},\gamma)^7$Be reaction was previously studied in this laboratory using polarized protons at a beam energy of 80 keV by Laymon *et al.* [1]. The results were analyzing powers with values of zero (to within the errors) at all angles in contrast to the very large analyzing powers measured for angles near 90° for ^{7}Li$(\vec{p},\gamma_0)^8$Be at 80 keV [2,3]. The large analyzing power observed in the ^{7}Li$(\vec{p},\gamma_0)^8$Be reaction indicated significant *p*-wave contributions at that low energy, attributed to the influence of nearby states in ^{8}Be [3]. The zero analyzing power for ^{6}Li$(\vec{p},\gamma)^7$Be was taken as evidence for the predominance of *s*-wave capture effects in that reaction [1]. Subsequently, the energy dependence of the low-energy astrophysical *S* factor for the ^{7}Li$(\vec{p},\gamma_0)^8$Be reaction was measured by Spraker *et al.* [4]. Those measurements showed that the astrophysical *S* factor increases as the proton energy decreases below 100 keV, producing a negative slope with energy.

Negative slopes for low-energy *S* factors are known to occur in situations where the particle binding energy of the final state is very small due, essentially, to the extended tail of the final (weakly bound) state wave function. This phenomenon, observed in the cases of ^{7}Be$(p,\gamma_0)^8$B and ^{16}O$(p,\gamma_1)^{17}$F, was discussed in the recent papers by Mukhamedzhanov and Nunes [5] and Jennings *et al.* [6]. However, the proton binding energy of the ground state of ^{8}Be is 17.26 MeV so that another reason must be the cause of the negative slope for ^{7}Li$(p,\gamma_0)^8$Be. Spraker *et al.* explained this negative slope of the *S* factor as due to the influence of a subthreshold state in ^{8}Be. A negative slope at low energy for the *S* factor of the ^{7}Li$(p,\alpha)^4$He reaction [7,8] has been shown to be caused by electron screening of the target nucleus.

The situation for ^{6}Li$(p,\gamma_0)^7$Be and ^{6}Li$(p,\gamma_1)^7$Be is intermediate between ^{7}Li$(p,\gamma_0)^8$Be and ^{7}Be$(p,\gamma_0)^8$B or ^{16}O$(p,\gamma_1)^{17}$F because the proton binding energies of the ground and first excited states in ^{7}Be are 5.61 MeV and 5.18 MeV, respectively. Also there are no states in ^{7}Be close enough to the region of excitation energy reached by low-energy proton capture on ^{6}Li (see Fig. 1) which could be expected to have any significant effect. Cecil *et al.* [9] measured the branching ratio of ^{6}Li$(p,\gamma_0)^7$Be and ^{6}Li$(p,\gamma_1)^7$Be with respect to ^{6}Li$(p,\alpha)^3$He from 45 to 170 keV and deduced the *S* factors for ^{6}Li$(p,\gamma_0)^7$Be and ^{6}Li$(p,\gamma_1)^7$Be as a function of energy. Their results gave a positive slope for the *S* factor. Switkowski *et al.* [11] measured the ^{6}Li$(p,\gamma)^7$Be cross section from 160 to 1150 keV. Their data points are all at energies above the present data set and show an *S* factor that increases with increasing energy. Barker's analysis [10] of the data of Switkowski *et al.* does have a negative *S*-factor slope for ^{6}Li$(p,\gamma_0)^7$Be and ^{6}Li$(p,\gamma_1)^7$Be at energies below the range of the data. The present measurements were under-

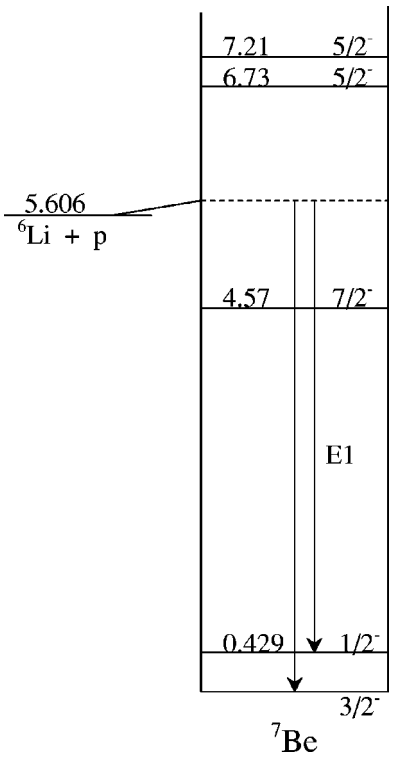

FIG. 1. Energy diagram of the known lower-energy states [12] in ^{7}Be showing the gamma transitions observed in the present experiment.

taken to examine this discrepancy in the previous measurements of Cecil *et al.* and Switkowski *et al.* and to look at a reaction where the binding energy of the final state is intermediate between 0.1 MeV and 17.3 MeV.

II. EXPERIMENTAL METHOD

The experimental setup was the same as that used by Spraker *et al.* [4] and will be described only briefly here. The TUNL atomic-beam-polarized ion source produced an 80-keV beam of protons. The proton beam was then further accelerated by biasing the target with a negative high voltage. Beam currents were typically 20–30 μA on target. Two separate data runs were made, one with target-bias voltages of 0, −15, and −30 kV and a second with voltages of −30, −40, and −50 kV. This produced data for beam energies of 80, 95, and 110 keV for the first run and 110, 120, and 130 keV for the second. During each run the target voltages were controlled by the data acquisition system such that the time spent at each bias voltage produced approximately the same number of counts. The time for a complete cycle of voltages was about 10 min so that effects due to changes in beam current or target conditions were minimized over the course of a typical 12-h run. Because of the high voltage on the target, the beam current was not integrated and the times at each voltage were used for normalization of the different energy data points within a given data set. The two data sets were normalized together at the 110-keV points.

The target was produced by an *in situ* evaporator in the target vacuum chamber. A shielded tungsten boat, which could be moved in front of the 3-mm-thick aluminum target backing, was used to evaporate enriched ^{6}Li (99%) onto the backing. The target was replenished approximately twice daily during the weeklong data runs. The lithium layer which was deposited was thick enough to stop the proton beam. Target conditions were monitored by observing the counting rate as a function of time.

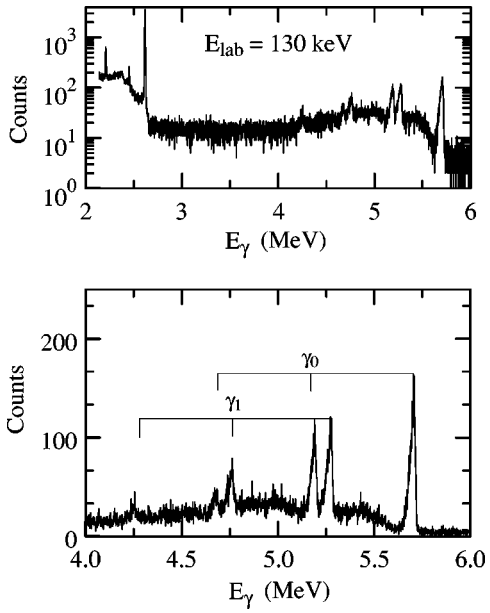

FIG. 2. Gamma-ray spectrum obtained with 130-keV protons. The top of the figure shows the spectrum above 2 MeV. The bottom shows the expanded region of interest and shows the broadening of the peaks due to the protons slowing in the target.

The gamma rays from the $^{6}\mathrm{Li}(p,\gamma_0)^{7}\mathrm{Be}$ and $^{6}\mathrm{Li}(p,\gamma_1)^{7}\mathrm{Be}$ reactions were detected by two large high-purity germanium detectors (123% and 140% efficient relative to $3''\times 3''$ NaI). The detectors were positioned at 90° on either side of the target chamber. The data acquisition system sorted the spectra for each detector according to target bias voltage and the beam polarization, which was switched between spin-up and spin-down configurations at a frequency of 10 Hz.

III. DATA ANALYSIS

A. Extracting yields from spectra

A gamma-ray spectrum obtained using 130-keV protons is shown in Fig. 2. The full energy peaks and the first and second escape peaks for the ground-state and first-excited-state gamma rays are indicated in the figure. The broadening of the low-energy sides of the peaks is due to events generated by protons which have lost energy as they stop in the thick target.

The yield of each spectrum was obtained by fitting a linear background to the region on each side of the peak. The yield was the sum of the counts in the peak with the linear background subtracted. The yields of the full-energy peaks and the first-escape peaks for the $^{6}\mathrm{Li}(p,\gamma_0)^{7}\mathrm{Be}$ and $^{6}\mathrm{Li}(p,\gamma_1)^{7}\mathrm{Be}$ reactions were extracted for each spectrum. As a result of the energy cycling procedure, spectra at different

energies in each of the two data sets were obtained with the same beam and target conditions. This made it possible to obtain the energy-dependent yields by normalizing the data to the same acquisition time. The results from the two separate data sets were normalized together using the overlapping data at a proton energy of 110 keV. The statistical uncertainties of the yields (including background subtraction) were included in the normalization process. It was assumed that the gamma rays were emitted isotropically in agreement with the measurements of Laymon *et al.* [1].

The yields from the ground-state and first-excited-state transitions can be used to calculate the branching ratio for these transitions. The ratio of the efficiencies of the detectors at 5.29 and 5.72 MeV is 1.053 ± 0.027 [12]. Using this and the ratios of the net counts in the two peaks, the ratio of the first-excited-state yield to the ground-state yield is 0.577 ± 0.017. This results in branching ratios of $(63.4 \pm 1.9)\%$ and $(36.6 \pm 1.9)\%$ for the ground-state and first-excited-state transitions, respectively. Within the uncertainties of the individual spectral yields, these ratios were constant over the energy range of this experiment. These are consistent with the values from Ref. [9] of 0.60 and 0.40, the values from Ref. [11] of $(59 \pm 3)\%$ and $(41 \pm 3)\%$, and the values of 62% and 38% in Ref. [13].

B. Obtaining the slope of the *S* factor

Values of the *S* factor could not be extracted from the yields at each beam energy because the beam current was not integrated, but the slope of the *S* factor could be extracted by fitting the integrated yields obtained at the incident beam energies of 80, 95, 110, 120, and 130 keV.

Since the proton beam stops in the target, the measured yield is the total yield from beam energy to zero. This yield can be written as

$$Y(E_p) = C \int_{E_p}^{0} \frac{\sigma(E) f}{\epsilon(E)} dE, \tag{1}$$

where E_p is the proton beam energy, $\sigma(E)$ is the energy-dependent cross section, f is the atomic fraction of the target, and $\epsilon(E)$ is the stopping power of the target for protons. The constant C includes the total number of incident protons and the detector solid angle and efficiency. In the present measurements this constant is proportional to the time spent at each value of the target bias voltage. The cross section can be written in terms of the astrophysical *S* factor as

$$\sigma(E_{\text{c.m.}}) = \frac{S(E_{\text{c.m.}})}{E_{\text{c.m.}}} e^{-2\pi\eta}, \tag{2}$$

where η is the Sommerfeld parameter and $2\pi\eta = 31.29 Z_1 Z_2 (\mu / E_{\text{c.m.}})^{1/2}$. Here Z_1 and Z_2 are the projectile and target charges, respectively, μ is the reduced mass in amu, and $E_{\text{c.m.}}$ is the center-of-mass energy in keV. The energy dependence of the *S* factor at the low energies of this experiment was assumed to be linear:

$$S(E_{\text{c.m.}}) = S_0 (1 + S_1 E_{\text{c.m.}}). \tag{3}$$

Using this form for the *S* factor puts all of the data normalization factors into the constant S_0 and puts the unknown energy-dependent part of the cross section in the constant S_1. The yield for a given beam energy can be calculated from Eq. (1) using the values of S_0 and S_1.

To compare the measured and calculated yields, the integral was evaluated numerically. The target was divided into 1-μg/cm^2 layers, each of which corresponds to an energy loss of less than 1 keV in the target material. The stopping power of the target was calculated using the energy loss equations of Anderson and Ziegler [14]. The yield for the first layer was then calculated using arbitrary starting values of S_0 and S_1. The energy loss for the layer was calculated, and the yield calculation was repeated for the next layer at the decreased energy. This process was repeated until the yield of a layer was less than 0.1% of the yield for the first layer. The total yield at that beam energy was the sum of the yields from all the layers of the target. This process was performed for all five beam energies and repeated iteratively, adjusting the values of S_0 and S_1 until a best fit to the data was obtained. The uncertainties in the values of S_1 were obtained from the error matrix of the fit [15] and thereby from the statistical uncertainties associated with experimental yields and included the effects of background subtraction.

The target material is believed to be Li_2O due to oxidation of the evaporated lithium metal due to residual oxygen in the vacuum system as discussed below. In the fitting procedure the target was assumed to be Li_2O. Other possibilities are that the target could have been pure Li or LiOH (due to water vapor in the vacuum system). The latter case is unlikely because of a liquid-nitrogen cold trap less than a meter from the target. The fitting procedure was repeated, assuming that the target composition was either pure lithium or LiOH. The extracted values for S_1 were identical to the value obtained when the target was assumed to be Li_2O.

The supposition that the target is Li_2O is supported by different observations. In the experiment of Spraker *et al.* on the ^{7}Li$(p,\gamma)^8$Be reaction, the ^{7}Li$(p,\alpha)^8$Be was also observed. Its much higher cross section allowed for the observation of variation of the yield over a short time span. During that experiment the counting rate decreased rapidly in the first several minutes after a new target was evaporated, leveled off at 40–45 % of the initial rate, and then stayed constant at that reduced rate for many hours. Calculations of the yield integral show that the ratio of yields for a thick $^6Li_2O$ target to a thick pure ^{6}Li target is 0.433. This indicates that the target was completely oxidized very soon after being evaporated and exposed to the beam and remained the same for many hours. This calculated ratio of yields is independent over a wide range of values of S_0 and S_1 used in the calculation. It was also noticed that the nearly opaque, reflective layer of Li metal which was deposited on the viewing window of the target chamber during each evaporation of a new target changed to a nearly transparent form within several minutes after a new evaporation, indicating a change in chemical composition.

C. Analyzing power data

The first data set at 80, 95, and 110 keV used the unpolarized beam from the TUNL atomic beam polarized ion

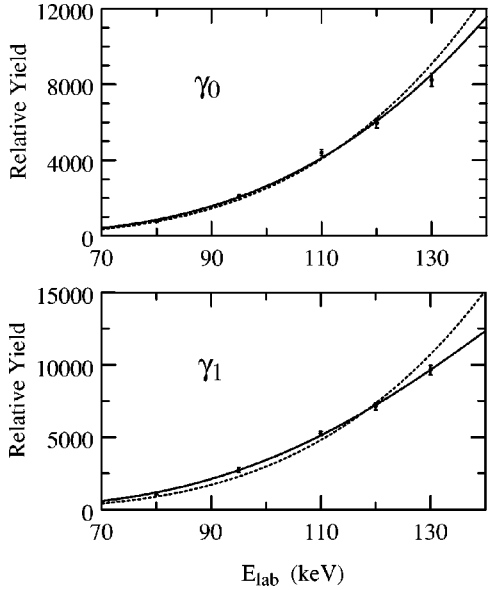

FIG. 3. Measured yields for $^6\mathrm{Li}(p,\gamma_0)^7\mathrm{Be}$ and $^6\mathrm{Li}(p,\gamma_1)^7\mathrm{Be}$. The error bars indicate the statistical uncertainty. The dashed lines are the calculated fits assuming the *S* factor is constant. The solid lines are the calculated fits assuming the *S* factor varies linearly with proton energy.

source so that no analyzing power data were taken during that run. For the second data set at 110, 120, and 130 keV the proton beam was polarized alternately in two different spin states. The beam was switched between the two spin states at a rate of 10 Hz. The beam polarization in each state was measured by the spin-filter technique [16]. The beam polarizations in the two states were 0.60 ± 0.05 and 0.77 ± 0.05. The data at each beam energy were sorted into separate spectra for each spin state. Using the procedure described above, the yields were extracted for each spin state at each beam energy. From the yields for the two spin states at 90°, the analyzing power was then calculated using

$$A_y = \frac{(Y_1 - Y_2)}{(p_2 Y_1 + p_1 Y_2)}, \tag{4}$$

where Y_1 (Y_2) corresponds to the yield for spin-up (down) protons and where p_1 and p_2 are the beam polarizations for the respective spin states.

IV. EXPERIMENTAL RESULTS

A. Slope of the *S* factor

The measured yields as a function of beam energy are shown in the top half of Fig. 3 for the ground-state transition. The error bars give the statistical uncertainty in the yields. The two curves shown are the best fits to the results assuming that the *S* factor is constant with energy (dashed curve) and that the *S* factor varies linearly with energy (solid curve). The solid curve clearly represents the data better. For this curve the slope parameter S_1 is -0.0037 ± 0.0009 keV^{-1}. The results for the first-excited-state transition are shown in the bottom of Fig. 3. The two curves are again the best fits to the data with the same notation as above. The value of S_1 for the solid curve is -0.0060 ± 0.0005 keV^{-1}. The uncertainties in S_1 are obtained from the error matrix of the fit [15].

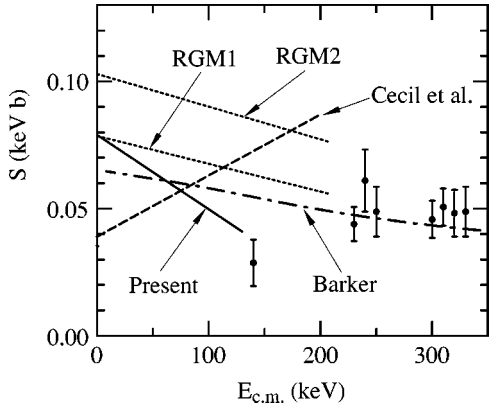

FIG. 4. The result of the present measurement (solid line) along with the previous results of Ref. [9] (dashed line) and Ref. [12] (dash-dotted line). The resonating group calculations are shown as the dotted lines. The data points shown are from Ref. [11].

The value of S_0 could not be extracted from the present measurements because the target biasing prevented integration of the incident beam. Laymon *et al.* [1] used a very similar apparatus for an 80-keV beam on a thick target and determined a value of $S_0 = 0.0269\pm0.0054$ keV b. However, in their analysis they assumed a constant *S* factor below 80 keV and assumed a pure ^{6}Li target despite the fact that the target was evaporated remotely and then transferred to the target chamber. Their value must thus be corrected for both of these effects. If the S_1 discussed above is used, their value of S_0 is increased by a factor of 1.277. Accounting for the lower yield of a Li_2O target increases S_0 by an additional factor of 2.288. These corrections change S_0 to 0.079 ± 0.018 keV b. Because of the similarity of techniques in the two experiments, this value has been adopted for the present experimental results.

Figure 4 shows the results of the present measurement along with the previous results for $^6\mathrm{Li}(p,\gamma_0)^7\mathrm{Be}$. The solid line is the present result obtained from the analysis discussed above. The dashed line is the result from Cecil *et al.* [9]. The data points shown are the lower-energy data of Switkowski *et al.* [11]. The result of Barker's [12] fit is the dash-dotted line. The dotted lines, labeled RGM1 and RGM2, are the results of the new resonating group calculations discussed later.

B. Analyzing power results and discussion

The analyzing powers at 90° determined at 110, 120, and 130 keV are shown in Fig. 5 for the ground-state and first-excited-state transitions. The error bars are due to statistical uncertainties and uncertainties in the beam polarization. The results are consistent with zero at all three energies. In the previous measurements of Laymon *et al.* [1] at 80 keV, the analyzing powers were also zero at all angles between 0° and 120°. Their analysis concluded that the *p*-wave contribution to the total cross section was $0.11\%\pm0.13\%$. The present

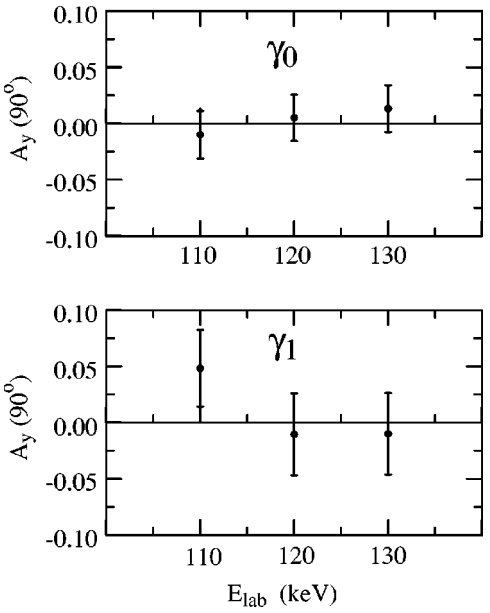

FIG. 5. Measured analyzing powers for $^6\mathrm{Li}(p,\gamma_0)^7\mathrm{Be}$ and $^6\mathrm{Li}(p,\gamma_1)^7\mathrm{Be}$. The error bars include the statistical uncertainties and the uncertainties in the beam polarization.

analyzing power results support the conclusion that the $^6\mathrm{Li}(p,\gamma)^7\mathrm{Be}$ reaction proceeds entirely by *s*-wave capture and *E*1 radiation.

V. DISCUSSION AND CALCULATIONS

A. *S*-factor slopes

The experimental slope parameter S_1 was determined to be negative for both the $^6\mathrm{Li}(p,\gamma_0)^7\mathrm{Be}$ and $^6\mathrm{Li}(p,\gamma_1)^7\mathrm{Be}$ reactions. The actual slope of the *S* factor with energy is the product of S_0 and S_1, where S_0 is the value of *S* at zero energy. The slope for $^6\mathrm{Li}(p,\gamma_1)^7\mathrm{Be}$ cannot be calculated since S_0 was not extracted for that reaction. For the $^6\mathrm{Li}(p,\gamma_0)^7\mathrm{Be}$ reaction, the slope is -0.00029 ± 0.000096 b. The slope from Barker's fit [10] to the data of Ref. [11] is -0.00016 b for $^6\mathrm{Li}(p,\gamma_0)^7\mathrm{Be}$, about half the present value. The value of S_0 from Barker's analysis is 0.0643 keV b, compared with the present value of 0.079 keV b. The data of Cecil *et al.* [9] showed an *S* factor increasing with energy (slope $=+0.00024$ b) in contradiction with the present data. Those data do give a value of 0.039 keV b for S_0, about half the present value. Their data for $^6\mathrm{Li}(p,\gamma_1)^7\mathrm{Be}$ also give a positive slope of 0.00016 b. Cecil *et al.* measured the branching ratio of the $^6\mathrm{Li}(p,\gamma_0)^7\mathrm{Be}$ and $^6\mathrm{Li}(p,\gamma_1)^7\mathrm{Be}$ yields with respect to the yield of the $^6\mathrm{Li}(p,^3\mathrm{He})^4\mathrm{He}$ reaction, rather than directly as for the present data and the data of Switkowski *et al.* [11].

B. Direct-capture calculations

Simple direct-capture calculations were made with the code HIKARI [17]. The bound-state wave function was calculated assuming the state consisted of a proton bound in the Woods-Saxon potential of the target nucleus. The depth of this potential was adjusted to give the observed binding energy of the final state. Because of the low proton energies, incident plane waves (with Coulomb distortions) were assumed. Although *E*1, *M*1, and *E*2 direct-capture terms were included, the calculated cross section was dominated in all cases by *s*-wave *E*1 radiation in agreement with the observation above that the measured analyzing powers indicate that only *s*-wave absorption occurs below 130 keV. Similar calculations performed for the $^7\mathrm{Be}(p,\gamma_0)^8\mathrm{B}$ and $^{16}\mathrm{O}(p,\gamma_1)^{17}\mathrm{F}$ reactions were able to reproduce the observed negative slopes in those reactions. However, the calculated slopes for $^7\mathrm{Li}(p,\gamma_0)^8\mathrm{Be}$, $^6\mathrm{Li}(p,\gamma_0)^7\mathrm{Be}$, and $^6\mathrm{Li}(p,\gamma_1)^7\mathrm{Be}$ are all zero for these direct-capture calculations. In summary, this simple direct-capture model cannot reproduce the observed values of S_1 for the $^7\mathrm{Li}(p,\gamma_0)^8\mathrm{Be}$, $^6\mathrm{Li}(p,\gamma_0)^7\mathrm{Be}$, and $^6\mathrm{Li}(p,\gamma_1)^7\mathrm{Be}$ reactions.

Barker [10] calculated cross sections for neutron and proton capture by $^6\mathrm{Li}$ by means of a direct-capture potential model and compared the results with experimental data. His calculations were different from the present direct-capture calculation in that different potentials were used for different incident partial waves and in that the analysis covered a much wider energy range than considered in the present work. Barker determined the parameters of the *s*-wave scattering potential by adjusting them in order to fit the complex scattering length determined from measurements of $^6\mathrm{Li}+n$ reactions. The results of this procedure produced a potential having a very small real-potential depth (23.63 MeV) and a large surface-absorption-potential depth (11.11 MeV). The bound-state potential had the same real depth and radius used in the Hikari calculations described above. Barker's fits agreed fairly well with the $^6\mathrm{Li}(p,\gamma)^7\mathrm{Be}$ data of Switkowski *et al.* [11] over the energy range from 200 keV to 1200 keV although the calculated cross sections were about a factor of 2 higher than the lowest-energy data point.

The code HIKARI assumes the same optical-model potential for all partial waves. However, in the proton energy range below 130 keV the reaction is dominated by *s*-wave absorption so that the optical-model potential for the code HIKARI could be taken to be Barker's *s*-wave potential. The result of this calculation produced an *S* factor having a small negative slope. The value of S_1 was -0.0016, a factor of 2 smaller than the present experimentally determined value but in agreement with Barker's calculated value. Barker's scattering potential parameters were also used in an optical-model calculation of the $^6\mathrm{Li}+p$ reaction in which the total-reaction cross section σ_T was calculated. The calculated value of the total-reaction cross section for this potential at proton energies between 100 and 200 keV is about 4 times larger than the accepted experimental cross section of the $^6\mathrm{Li}(p,\alpha)^3\mathrm{He}$ reaction [18], which dominates σ_T.

Further searches of the potential parameter space could produce even better fits to the data. However, the physical meaning of the parameters thus obtained is not clear. The problem is more likely in the simplicity of the model itself. A multichannel model that explicitly includes all of the open reaction channels and a more realistic representation of the $^7\mathrm{Be}$ ground state seem to be needed here.

C. Effects of nearby states

As previously mentioned, the calculated slope using the direct-capture model was found to be zero in the case of the ^{7}Li$(p,\gamma_0)^8$Be reaction. The observed negative value of S_1 was, in that case, reproduced by the inclusion of a 2^+ subthreshold state in ^{8}Be [4]. The large analyzing power for ^{7}Li$(p,\gamma_0)^8$Be has also been shown to be due to 1^+ states in ^{8}Be at energies a few hundred keV above the excitation region studied [3]. The possibility of explaining the negative S_1 for ^{6}Li$(p,\gamma)^7$Be in a similar manner was considered. An energy diagram of the known lower energy states [12] in ^{7}Be is shown in Fig. 1. The excitation region studied is more than 1 MeV from the nearest known state in ^{7}Be. Additionally, the nearest states have spins and parities of either $7/2^-$ or $5/2^-$. The $7/2^-$ state could only be produced by the absorption of f-wave incident protons, and the $5/2^-$ states could only be produced by the absorption of p-wave or f-wave protons. Decay to the ground state would then produce $M1$ or higher multipole radiation. A significant $M1$ amplitude would be expected to interfere with the s-wave $E1$ amplitude and produce a nonzero analyzing power at 90° in conflict with the measured analyzing power. It is therefore concluded that the effects of other known states in ^{7}Be could not account for the observed negative value of the S_1 parameter.

D. Effects of electron screening

There have been measurements of low-energy cross sections for various light elements from which the effects of atomic electron screening have been deduced (see Ref. [8] and references therein). The standard form for the astrophysical S factor as defined in Eq. (2) above transforms the cross section into a form where the s-wave Coulomb penetrability is factored out, leaving the presumably slowly varying S factor. This treatment assumes a projectile and target nucleus with no electron clouds present: i.e., bare nuclei. At low energies this is not a valid approximation for the usual experimental situation [7]. The effective repulsion between the projectile and target is reduced by the electron screening effects, increasing the low-energy cross section. This can be described by an enhancement factor [8]

$$f_{\rm lab}(E) = \frac{\sigma_s(E)}{\sigma_e(E)} = \exp\left(\frac{\pi\eta U_e}{E}\right), \tag{5}$$

where $\sigma_s(E)$ and $\sigma_e(E)$ refer to the cross sections for electron-shielded and bare nuclei, respectively. The Sommerfeld factor is η, and U_e is the electron screening potential energy [7], which is the difference in the electron binding energies of the atoms in the entrance channel and of the composite atom in the adiabatic limit. Lattuada *et al.* used the Trojan horse method [8] to extract the bare-nucleus S factor for the ^{7}Li$(p,\alpha)^4$He reaction. From this they empirically determined a value for the electron-screening potential energy, $U_e = 330 \pm 40$ eV, for protons incident on ^{7}Li. This value of U_e has been used with Eq. (4) above to estimate the effects of electron screening on the S factor for ^{6}Li$(p,\gamma)^7$Be. In the present experiment the protons striking the target slow down from the beam energy to zero within the target. However, most of the yield occurs for the higher energies in the target because the cross section decreases exponentially with decreasing proton energy. Table I shows the calculated energies at which 50% of the yield has been produced (E_{50}) and at which 90% of the yield has been produced (E_{90}). From Eq. (5) it is possible to calculate the slope of the cross section ratio, which is the same as the slope of the S factor at a specific energy. Table I shows this slope in the last two columns; the slopes are evaluated at the energies E_{50} and E_{90}. If the bare-nucleus S factor is assumed to be constant with energy as indicated by the direct-capture calculations, then the S-factor slopes in Table I are the slopes of the electron-screened S factor at the indicated energies and can be compared directly with the value of S_1 extracted in the present experiment (-0.0037 ± 0.0009 keV^{-1}). It can be seen that the experimental value is about an order of magnitude larger than the calculated values so that electron screening effects are not large enough to explain the present data.

TABLE I. E_{50} and E_{90} are the calculated proton energies at which the yield is 50% and 90% complete. $S_1(50)$ and $S_1(90)$ are the values of the S_1 slope parameter due to electron screening at the energies E_{50} and E_{90}. The value of S_1 from the present data is -0.0041 ± 0.0009 keV^{-1}.

Beam energy (keV)	E_{50} (keV)	E_{90} (keV)	$S_1(50)$ (keV^{-1})	$S_1(90)$ (keV^{-1})
80	71.5	55.5	−0.00044	−0.00086
95	84.1	64.2	−0.00029	−0.00058
110	96.7	72.6	−0.00020	−0.00042
120	104.9	77.9	−0.00016	−0.00035
130	113.2	83.3	−0.00013	−0.00030

E. Resonating-group-model calculations

The astrophysical S factors for the reactions ^{4}He$(^3$H$,\gamma)^7$Li and ^{4}He$(^3$He$,\gamma)^7$Be were calculated in the framework of the resonating group model in Ref. [19] [referred to subsequently as Mertelmeier and Hofmann (MH)]. The calculated values agreed reasonably well with the data when the coupling to the closed channels ^{6}Li-nucleon was taken into account. Simple wave functions for the fragments ^{3}H, ^{3}He, ^{4}He, and ^{6}Li were used for these calculations. These calculations have now been extended to describe the radiative capture reaction ^{6}Li$(p,\gamma)^7$Be in the presence of the open ^{3}He-α channel.

For this calculation (RGM1) the simple wave functions for ^{3}He and α, given implicitly in the ^{7}Li wave functions in Appendix 2 of MH, were used. They consisted of one width parameter for the α and two for the ^{3}He. For the ^{6}Li ground state the pure s-wave part as given in Eq. (A14) of MH was used. For the radial wave functions between the fragments, 20 width parameters similar to those given below Eq. (22) of MH were used. This simple model predicts the ^{7}Be ground state 1.5 MeV below the α-^{3}He threshold and the ^{6}Li-p threshold 5.3 MeV above the α-^{3}He threshold. The bound-state wave function in the capture calculation included all the

20 radial width parameters. Using the effective nucleon-nucleon force as given in Appendix 3 of MH, only the $E1$ s waves contribute below 1 MeV $E_{\mathrm{c.m.}}$ to the $^6\mathrm{Li}+p$ capture with the $^2S_{1/2}$ dominating and the $^4S_{3/2}$ being a 5% correction. All the other partial waves and the multipolarities $E2$ and $M1$ are well below the one percent level. The value of the S factor actually reproduces the value adopted in this work and, as shown in Fig. 4, a negative slope, albeit somewhat smaller than observed.

Since the ^{6}Li-p threshold was calculated to be about 1 MeV higher than in nature, a second calculation (RGM2) which reproduces this threshold much better was used to estimate the uncertainties in this simple model. For this purpose the wave functions determined for the scattering calculation in Ref. [20] were used for the fragments—namely, two width parameters for ^{3}He and α and, for the ^{6}Li, an α-deuteron configuration with s waves and d waves on the relative coordinate, one width parameter for the internal α and deuteron, and two width parameters on the α-deuteron coordinate (for details, see the Appendix of Ref. [20]). The same radial parameters as above were taken here. The calculated ^{6}Li-p threshold of +4.05 MeV relative to ^{3}He-^{4}He and the calculated ground-state energy of −1.33 MeV are close to the experimental values.

The calculated S-factor values from RGM2 are quite a bit higher than for the first calculation. This is due to the smaller width parameter used for the ^{6}Li wave function. This leads to a bigger rms radius and thus to a larger cross section at low energies since the particles touch each other earlier. The behavior of the S factor with energy is almost the same for RGM1 and RGM2. The value of S_1 of Eq. (3) was found to be -0.0013 keV^{-1} for RGM1 and -0.0015 keV^{-1} for RGM2, as compared with the experimental value of -0.0037 ± 0.0009.

The S factors from both calculations are shown in Fig. 4. In both cases the S factor falls with increasing energy. This fact was also found for the capture reactions $^4\mathrm{He}(^3\mathrm{H},\gamma)$ and $^4\mathrm{He}(^3\mathrm{He},\gamma)$ and is attributed to the s-wave scattering phase shifts also falling with energy [see Figs. 8 and 9(a) of Ref. [19]]. The falling scattering phase shifts are due to the underlying Pauli-forbidden state in this channel. It is the coupling to the strong $^6\mathrm{Li}(p,\alpha)$ channel which gives rise to this result. Only a coupled-channel calculation is able to generate the negative slope arising from this effect.

The calculated values are only in fair agreement with the data. Unfortunately, the crude model cannot easily be improved, as the complicated ^{6}Li wave function studied in MH, which reproduced all bound-state properties very well, yields a binding energy close to the α-^{3}He threshold. Since this threshold can only be lowered by a more realistic potential, such a calculation is out of reach at the moment.

VI. CONCLUSIONS

The energy dependence of the astrophysical S factor has been extracted for the $^6\mathrm{Li}(p,\gamma_0)^7\mathrm{Be}$ and $^6\mathrm{Li}(p,\gamma_1)^7\mathrm{Be}$ reactions for proton energies below 130 keV. The results are S factors that decrease significantly with increasing energy. Explanations in terms of the binding energy of the final state, nearby states in the final nucleus, and electron-screening effects all fail to reproduce these results. The calculations of Barker [10] do produce a negative slope but predict values of other observables (e.g., the low-energy capture cross section and the total reaction cross section) which are in conflict with the results of previous experiments. A more detailed microscopic multichannel calculation does reproduce the sign of the slope. This calculation establishes the fact that coupling to other strong channels can give rise to a negative slope of the S factor in a (p,γ) reaction, a new mechanism which should be taken into account when extrapolating S factors into the astrophysically relevant energy region.

ACKNOWLEDGMENTS

This work was partially supported by grants from the U.S. Department of Energy under Grants Nos. DE-FG02-97ER41046, DE-FG02-97ER41033, and DE-FG02-97ER41042.

[1] C. M. Laymon, R. M. Prior, D. R. Tilley, and H. R. Weller, Phys. Rev. C **53**, 1977 (1996).
[2] R. M. Chasteler, H. R. Weller, D. R. Tilley, and R. M. Prior, Phys. Rev. Lett. **72**, 3949 (1994).
[3] M. A. Godwin, C. M. Laymon, R. M. Prior, D. R. Tilley, and H. R. Weller, Phys. Rev. C **56**, 1605 (1997).
[4] M. Spraker, R. M. Prior, M. A. Godwin, B. J. Rice, E. A. Wulf, J. H. Kelley, D. R. Tilley, and H. R. Weller, Phys. Rev. C **61**, 015802 (2000).
[5] A. M. Mukhamedzhanov and F. M. Nunes, Nucl. Phys. **A708**, 437 (2002).
[6] B. K. Jennings, S. Karataglidis, and T. D. Shoppa, Phys. Rev. C **58**, 579 (1998), and references therein.
[7] H. J. Assenbaum, K. Langanke, and C. Rolfs, Z. Phys. A **A327**, 461 (1987).
[8] M. Lattuada, R. G. Pizzone, S. Typel, P. Figuera, D. Miljanic, A. Musumarra, M. G. Pellegriti, C. Rolfs, C. Spitaleri, and H. H. Wolter, Astrophys. J. **562**, 1076 (2001), and references therein.
[9] F. E. Cecil, D. Ferg, H. Liu, J. C. Scorby, J. A. McNeil, and P. D. Kunz, Nucl. Phys. **A539**, 75 (1992).
[10] F. C. Barker, Aust. J. Phys. **33**, 159 (1980).
[11] Z. E. Switkowski, J. C. P. Heggie, D. L. Kennedy, D. G. Sargood, F. C. Barker, and R. H. Spear, Nucl. Phys. **A331**, 50 (1980).
[12] G. J. Schmid, R. M. Chasteler, C. M. Laymon, H. R. Weller, E. F. Moore, C. R. Bybee, J. M. Drake, D. R. Tilley, G. Vavrina, and P. M. Wallace, Nucl. Phys. **A607**, 139 (1996).
[13] F. Ajzenberg-Selove, Nucl. Phys. **A490**, 1 (1988).
[14] H. H. Anderson and J. F. Ziegler, *Hydrogen Stopping Powers and Ranges in All Elements* (Pergamon, London, 1977).
[15] P. R. Bevington and D. K. Robinson, *Data Reduction and Er-*

ror Analysis for the Physical Sciences (McGraw-Hill, New York, 2003).
[16] A. J. Mendez, C. D. Roper, J. D. Dunham, and T. B. Clegg, Rev. Sci. Instrum. **67**, 3073 (1996).
[17] H. Kitazawa, computer code HIKARI (unpublished), Triangle Universities Nuclear Laboratory Annual Report No. TUNL-XIX, 1980, p. 114.
[18] C. Angulo *et al.*, Nucl. Phys. **A656**, 3 (1999).
[19] T. Mertelmeier and H. Hofmann, Nucl. Phys. **A459**, 387 (1986).
[20] H. M. Hofmann and T. Mertelmeier, Nucl. Phys. **A410**, 208 (1983).